

Dense labeling of large remote sensing imagery with convolutional neural networks: a simple and faster alternative to stitching output label maps

Bohao Huang¹, Daniel Reichman¹, Leslie M. Collins¹, Kyle Bradbury², and Jordan M. Malof¹

¹Department of Electrical & Computer Engineering, Duke University, Durham, NC 27708

²Energy Initiative, Duke University, Durham, NC 27708

Abstract— In this work we consider the application of convolutional neural networks (CNNs) for pixel-wise labeling (a.k.a., semantic segmentation) of remote sensing imagery (e.g., aerial color or hyperspectral imagery). Remote sensing imagery is usually stored in the form of very large images, referred to as “tiles”, which are too large to be segmented directly using most CNNs and their associated hardware. As a result, during label inference, smaller sub-images, called “patches”, are processed individually and then “stitched” (concatenated) back together to create a tile-sized label map. This approach suffers from computational inefficiency and can result in discontinuities at output boundaries. We propose a simple alternative approach in which the input size of the CNN is dramatically increased *only during label inference*. This does not avoid stitching altogether, but substantially mitigates its limitations. We evaluate the performance of the proposed approach against a conventional stitching approach using two popular segmentation CNN models and two large-scale remote sensing imagery datasets. The results suggest that the proposed approach substantially reduces label inference time, while also yielding modest overall label accuracy increases. This approach contributed to our winning entry (overall performance) in the INRIA building labeling competition.

Index Terms— semantic segmentation, convolutional neural networks, deep learning, aerial imagery, building detection

I. INTRODUCTION

Convolutional neural networks (CNNs) have recently achieved groundbreaking results for the semantic segmentation (i.e., dense pixel-wise labeling) of remote sensing imagery, such as color or hyperspectral satellite imagery [1]–[12]. For example, performance in several recent benchmark problems has been dominated by CNNs including a recent Kaggle competition for building labeling [12], the INRIA building labeling competition [13], and the recent ISPRS labeling competition [14].

Here we consider the scenario in which we wish to infer pixel labels for a new image using a trained CNN. Raw remote sensing imagery is often stored as large image “tiles”, which cannot be processed directly because of limited memory on the graphics processing units (GPUs) used by modern CNNs. A common solution to this problem is to extract smaller

sub-images, termed patches, and process them individually. Once label maps are inferred for each patch, they are “stitched” (e.g., concatenated) together to form a tile-sized label map. This process is illustrated in Fig. 1. Among the authors that have reported their label inference approach, all authors (to our knowledge) report using some variant of this “stitching” approach [2], [3], [8]–[11].

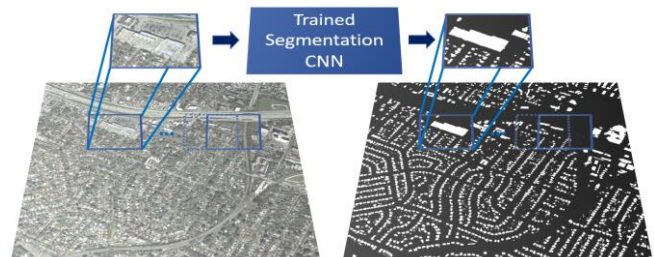


Fig. 1. Illustration of the process of stitching together large contiguous semantic label maps (right) using the output of smaller input patches extracted from the original imagery (left).

A. Challenges associated with label map stitching

While the stitching strategy shown in Fig. 1 has become popular, with many variants in the literature [2], [3], [8]–[11], it has several limitations. First, and foremost, it increases the time needed for inferring labels, which is a major consideration when processing massive remote sensing imagery data. This is largely due to the additional data handling needed to extract and stitch many patches from the larger image tiles.

Label stitching strategies are also complicated by the tendency of many CNN architectures (e.g., the DeepLab [15], and variants of U-net [16]) to have greater error rates at the edges of their output label maps. This was reported in [12] for the U-net model, and is reproduced here with our datasets, using two popular CNN architectures, in Fig. 2. We hypothesize in this work that this characteristic increases overall error rates in the label maps after stitching. This effect can be mitigated by extracting

patches more densely from tiles, so that they overlap, and then cropping the edges of the corresponding label maps. However, this strategy comes at the price of further increasing the computational costs (e.g., [12]) of stitching, and thereby further slowing label inference.

Finally, in addition to slower label inference, the stitching process also often yields label discontinuities at the boundaries of neighboring label maps (e.g., in [12]). Fig. 3(a) presents an example of this problem.

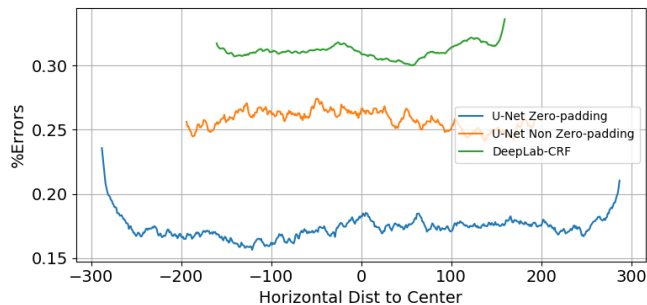


Fig. 2: Percentage of errors across patches for U-Net and Deeplab-CRF CNN models when applied to our INRIA dataset. The error percentage is normalized so that it will sum to 100. The standard U-net model differs from the Deeplab-CRF model because it uses no zero-padding (as indicated in the the legend) for its intermediate feature maps, while the Deeplab-CRF uses zero-padding throughout its feature layers. The Deeplab-CRF model has many layers, and the zero-padding is needed to maintain the spatial size of its output. The Deeplab-CRF *tends* to exhibit higher errors at its edges, while the U-net does not. We hypothesize that this is because of the deterioration in filter responses at the edges of feature maps when their input includes some zero-padding, ultimately reducing the quality of the output label maps. To investigate this further, we also evaluate a U-net with zero-padding in its intermediate feature layers, and we find that it exhibits substantial errors on the edges, suggesting that zero-padding does indeed contribute to this tendency.

B. Proposed alternative to image patch stitching

One easy way to reduce all of the aforementioned negative effects of label stitching is to increase the input-patch size of CNNs. Unfortunately, however, the input-patch size is often limited due to the memory available on a GPU. In particular, training a CNN requires substantial memory, which creates a major bottleneck for the feasible input-patch size of CNNs. In this work we propose to overcome this problem, and substantially reduce the negative impacts of label stitching, by artificially increasing the input-patch size of CNNs *only during label inference*.

Historically, the input-patch size of CNNs during training and label inference (a.k.a., testing) was constrained to be identical, making it impossible to make the size of the input patches larger once training is complete. However, since fully convolutional architectures were proposed in [17],

most modern CNN architectures, including those for semantic segmentation (e.g., [15], [16]), have become fully convolutional. This makes it possible to change the input-patch size of CNNs with relative ease. Despite this new capability, this approach remains unexplored in the research community.

In this work we aim to bring this approach to the attention of the research community, and conduct experiments to investigate its benefits using two popular segmentation CNN architectures applied to two large remote sensing datasets. We compare the proposed approach to a representative stitching approach employed in [12], [16]. The results suggest that the proposed approach substantially reduces the time needed for label inference, while also yielding modest increases in overall label accuracy. This approach was used in our winning entry in the recent INRIA building labeling competition [4], [13], and is an extension of our preliminary work on this [18].

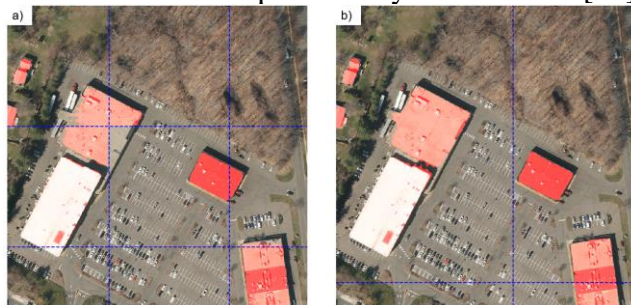


Fig. 3. Two examples of stitched building label maps created from the output of a segmentation CNN. The predicted building pixels are highlighted in red. In (a) the map is generated by stitching 321×321 patches. These smaller patches require more processing and increase the probability of edge effects, such as the discontinuity visible in the upper left of the center patch in (a); the predicted rooftop of neighboring patches is discontinued at the boundary with the middle patch. In (b) we employed the same network (i.e., on 321×321 patches), but we resized the output of the network to 736×736 during stitching, resulting in faster processing and a mitigation of the aforementioned edge effect.

II. THE REMOTE SENSING DATASETS

A. The INRIA building labeling dataset (D1)

Dataset 1 (D1) is the INRIA Aerial Image Labeling Challenge Dataset [13]. This dataset contains aerial RGB imagery collected from 10 cities in both the U.S. and Europe, however in this work, we only used the 5 cities with publicly available ground truth labeling: Austin, Chicago, Kitsap, Western Tyrol, and Vienna. A total of 36 images were captured over each city at a ground sampling rate of 0.3 m. Each of the 36 images encompasses 2.25 km^2 , which translates to 5000×5000 pixels in each tile.

B. The solar array labeling dataset (D2)

Dataset 2 (D2) is a color (RGB) dataset of orthorectified aerial photography for the problem of pixel-wise solar photovoltaic array labeling [19]. We used a subset of the data comprising roughly 19,000 solar arrays, over 1000 km² of area collected over three municipalities in California, U.S.A: Fresno, Modesto, and Stockton. This subset was chosen because all of the imagery was collected at the same 0.3-meter resolution. This dataset has been employed in several studies of semantic segmentation [20], [21].

III. NEURAL NETWORK ARCHITECTURES AND TRAINING DETAILS

In this work we used two popular semantic segmentation models: U-Net [16] and DeepLab-CRF [15]. We briefly review these architectures below.

A. The U-Net architecture

The U-net is a popular semantic segmentation CNN architecture [16] that was originally proposed for the segmentation of medical imagery in [16]. We use the U-net architecture as it was proposed in [16], with the single exception that we use half as many filters in each convolutional layer. This modification was adopted because it was used by the winning entry in the INRIA building labeling competition[13].

Note that the U-net model does not employ any zero-padding in its intermediate convolutional (feature) layers. Therefore, its output feature maps (and final label map) are smaller than its input. However, as we hypothesize in Fig. 2, this has the benefit of improving the accuracy of the U-nets label predictions at the edges of its output label maps.

B. The DeepLab-CRF architecture

The DeepLab models adapt Atrous Convolution to maintain the spatial extent of the output feature maps throughout convolutional layers. In [15], the DeepLab implementation based on the ResNet-101 architecture [22] was reported to outperform the implementation based on VGG16 [23] for the PASCAL-VOS 2012 dataset [24]. Therefore, we chose to utilize the DeepLab implementation with the ResNet-101 network architecture in our experiments. Since we are focusing on addressing stitching problems specifically associated with CNNs, we did not include the Conditional Random Field (CRF) often applied after post processing.

Note that, in contrast to the U-net model, the DeepLab-CRF model uses padding zero-padding throughout its intermediate convolutional (feature) layers in order to help maintain the spatial extent of its output label map. As we hypothesize in Fig. 2, this has the effect of reducing the accuracy of the label predictions of the Deeplab-CRF at the edges of its output label maps.

C. Network training

We trained both of the CNN models (DeepLab-CRF and U-Net) using D1 and D2. For D1, the first five tiles in each city formed the validation set and the remaining 31 tiles in each city were used for training. For D2, we used the first half of the images in each city as the validation set, and the used the remaining half as the training set.

The optimization procedure and the related parameter settings in all of the experiments are consistent across models. The optimization objective function is the discrete cross entropy cost, which is widely used [25]. Unless specified, we use a batch size of 5 and patch size of 572×572 pixels for the U-Net models (with no zero padding) and 321×321 pixels for the DeepLab-CRF models. An Adam optimizer [26] with $\beta_1 = 0.9$, $\beta_2 = 0.999$, $\epsilon = 10^{-8}$ is used. The models are trained for 100 epochs with 8,000 batches per epoch. For the experiments with the U-Net no zero-padding model, we trained the networks with a learning rate of 10^{-4} and dropped to 10^{-5} after 60 epochs. For the experiments with the DeepLab-CRF model, we trained them with a learning rate of 10^{-5} and dropped to 10^{-6} after 60 epochs.

IV. EXPERIMENTS

A. Experimental design details

For both of the segmentation models in our experiments we increased the image input patch size as large as possible during label inference (limited only by the memory of our GPUs). To infer the pixel-wise predictions of an entire 5000×5000 tile, we extract smaller image patches along a grid, and then stitch the output of the patches together. A final label is chosen for each pixel based upon the maximum predicted class probability at that pixel. The label predictions of the CNNs were scored using the widely used Intersection of Union (IoU) metric [24]. In our experiments, input patch sizes are increased

only during label inference. The input patch sizes for all networks did not change during training.

B. Computational time comparisons

The computational time for generating label predictions with the U-Net and the DeepLab-CRF models is shown in Fig. 5. The trend in performance is similar for both of the models that were considered: as the patch size increases, the running time decreases. The running time decreases due to (i) there is reduced redundancy in the convolutional operations among overlapping neighboring patches and (ii) because less stitching operations are required. The simplicity of this approach and its faster running time are likely its greatest advantages.

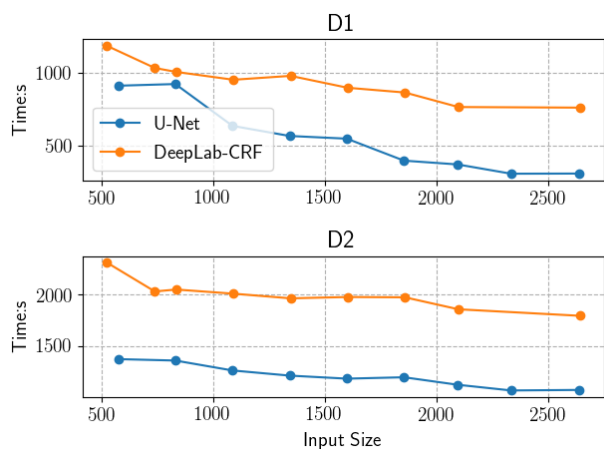


Fig. 4. Running time comparison for the U-Net and DeepLab-CRF generating label predictions on all of the images in the validation data set in D1 and D2. In each plot, the input size at testing is shown on the X-axis.

C. Label accuracy comparisons

In Fig. 6 we compare the segmentation performance of the U-Net and DeepLab-CRF models by measuring the IoU on validation images. For the DeepLab-CRF model, there is a large performance gain when increasing the input size at testing. As shown in Fig. 2, the DeepLab-CRF model generates poorer results at the boundary of input patch. By increasing the input patch size, the percentage of the output pixels impacted by this effect can be reduced, resulting in an overall performance improvement in the stitched output label maps.

Another more surprising experimental result is the small, but consistent, performance improvement the U-Net model as the patch size increases. We see in Fig. 2 that the U-net has similar errors across its output patch, and therefore a performance

improvement is surprising. We hypothesize that there may still be relatively higher error rates at the edges of its output, even though they are not apparent in Fig. 2 once zero-padding is removed.

In this work we hypothesize that zero-padding generally degrades any features extracted at the edges of feature maps in each layer of the CNN, which then ultimately lowers the accuracy of the output label maps at their edges. Our empirical results (here and Fig. 2) are consistent with this hypothesis, suggesting that CNNs employing greater zero-padding (e.g., DeepLab-CRF) benefit much more from the proposed approach. This is an important finding because most modern CNN architectures use some degree of zero-padding, including many of those achieving top performances on benchmark datasets [15], [22], [27], [28]. For these CNNs, our proposed approach can not only accelerate inference time but also improve performance.

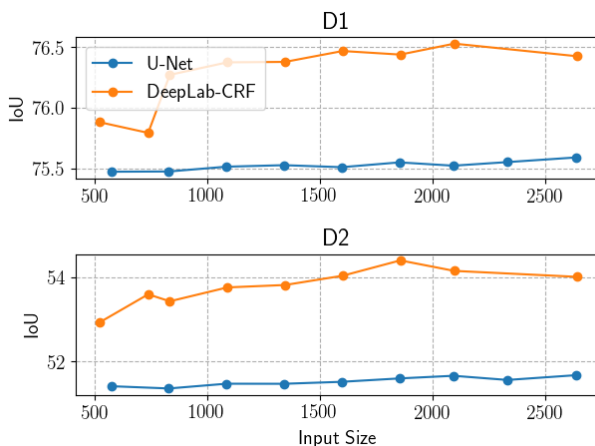


Fig. 5. IoU of U-Net and DeepLab-CRF on the validation data set from D1 and D2. In each plot, the input size at testing is shown on the X-axis.

V. CONCLUSIONS

In this work we proposed a simple approach that substantially mitigates the effects of “stitching” output label maps produced by CNNs for the segmentation of remote sensing imagery. Our approach involves increasing the input-patch size of the CNN *only during the label inference step*. The performance of the proposed approach was compared against a common stitching method using two popular segmentation CNN architectures and two large remote sensing datasets.

Our results indicate that the proposed method substantially reduces label inference time, which is a

key consideration with massive remote sensing datasets. The proposed method also modestly improves overall label accuracy. We suspect that the magnitude of the accuracy improvements depends upon the quantity of zero-paddings used within the convolutional layers of the CNN. Zero-padding is common among modern CNN architectures and we anticipate modest accuracy improvements in addition to reductions in computation time among most CNNs that adopt this approach for semantic labeling.

ACKNOWLEDGEMENTS

We thank the NVIDIA corporation for donating a GPU for this work, and the XSEDE and the Duke Compute Clusters for providing computing resources. We would also like to thank the Duke University Energy Initiative for supporting our work.

REFERENCES

- [1] Y. Liu, B. Fan, L. Wang, J. Bai, S. Xiang, and C. Pan, "Semantic labeling in very high resolution images via a self-cascaded convolutional neural network," *ISPRS J. Photogramm. Remote Sens.*, 2017.
- [2] D. Marmanis, K. Schindler, J. D. Wegner, S. Galliani, M. Datcu, and U. Stilla, "Classification with an edge: Improving semantic image segmentation with boundary detection," *ISPRS J. Photogramm. Remote Sens.*, vol. 135, pp. 158–172, 2018.
- [3] D. Marmanis, J. D. Wegner, S. Galliani, K. Schindler, M. Datcu, and U. Stilla, "Semantic Segmentation of Aerial Images With an Ensemble of Cnns," *ISPRS Ann. Photogramm. Remote Sens. Spat. Inf. Sci.*, vol. III-3, pp. 473–480, 2016.
- [4] B. Huang *et al.*, "Large-scale semantic classification: outcome of the first year of inria aerial image labeling benchmark," in *International Geoscience and Remote Sensing Symposium*, 2018.
- [5] A. Marcu and M. Leordeanu, "Dual Local-Global Contextual Pathways for Recognition in Aerial Imagery," 2016.
- [6] S. Paisitkriangkrai, J. Sherrah, P. Janney, and A. Van-Den Hengel, "Effective semantic pixel labelling with convolutional networks and Conditional Random Fields," *IEEE Comput. Soc. Conf. Comput. Vis. Pattern Recognit. Work.*, vol. 2015–Octob, pp. 36–43, 2015.
- [7] S. Piramanayagam, W. Schwartzkopf, F. W. Koehler, and E. Saber, "Classification of remote sensed images using random forests and deep learning framework," no. October 2016, p. 100040L, 2016.
- [8] H. Wang, Y. Wang, Q. Zhang, S. Xiang, and C. Pan, "Gated convolutional neural network for semantic segmentation in high-resolution images," *Remote Sens.*, vol. 9, no. 5, pp. 1–15, 2017.
- [9] J. Sherrah, "Fully Convolutional Networks for Dense Semantic Labelling of High-Resolution Aerial Imagery," pp. 1–22, 2016.
- [10] M. Volpi and D. Tuia, "Dense semantic labeling of subdecimeter resolution images with convolutional neural networks," *IEEE Trans. Geosci. Remote Sens.*, vol. 55, no. 2, pp. 881–893, 2017.
- [11] N. Audebert, B. Le Saux, and S. Lefèvre, "Semantic Segmentation of Earth Observation Data Using Multimodal and Multi-scale Deep Networks," 2016.
- [12] V. Iglovikov, S. Mushinskiy, and V. Osin, "Satellite Imagery Feature Detection using Deep Convolutional Neural Network: A Kaggle Competition," 2017.
- [13] E. Maggiori *et al.*, "Can Semantic Labeling Methods Generalize to Any City? The Inria Aerial Image Labeling Benchmark," pp. 3226–3229, 2017.
- [14] J. D. W. Franz Rottensteiner, Gunho Sohn, Markus Gerke, "ISPRS Test Project on Urban Classification and 3D Building Reconstruction," *ISPRS - Comm. III - Photogramm. Comput. Vis. Image Anal. Work. Gr. III / 4 - 3D Scene Anal.*, pp. 1–16, 2013.
- [15] L.-C. Chen, G. Papandreou, I. Kokkinos, K. Murphy, and A. L. Yuille, "DeepLab: Semantic Image Segmentation with Deep Convolutional Nets, Atrous Convolution, and Fully Connected CRFs," pp. 1–14, 2016.
- [16] O. Ronneberger, P. Fischer, and T. Brox, "U-Net: Convolutional Networks for Biomedical Image Segmentation," pp. 1–8, 2015.
- [17] J. Long, E. Shelhamer, T. Darrell, J. Long, and T. Darrell, "Fully Convolutional Networks for Semantic Segmentation ppt," *Proc. IEEE Conf. Comput. Vis. Pattern Recognit.*, vol. 39, no. 4, pp. 3431–3440, 2015.
- [18] B. Huang, L. M. Collins, K. Bradbury, and J. M. Malof, "Deep convolutional segmentation of remote sensing imagery: a simple and efficient alternative to output image stitching," in *International Geoscience and Remote Sensing Symposium*, 2018.
- [19] K. Bradbury *et al.*, "Distributed solar photovoltaic array location and extent dataset for remote sensing object identification," *Sci. data*, vol. 3, p. 160106, 2016.
- [20] J. M. Malof, K. Bradbury, L. M. Collins, and R. G. Newell, "Automatic detection of solar photovoltaic arrays in high resolution aerial imagery," *Appl. Energy*, vol. 183, 2016.
- [21] J. Camilo, R. Wang, L. M. Collins, K. Bradbury, and J. M. Malof, "Application of a semantic segmentation convolutional neural network for accurate automatic detection and mapping of solar photovoltaic arrays in aerial imagery," in *IEEE Applied Imagery Pattern Recognition Workshop*, 2017.
- [22] K. He, X. Zhang, S. Ren, and J. Sun, "Deep residual learning for image recognition," in *Proceedings of the IEEE conference on computer vision and pattern recognition*, 2016, pp. 770–778.
- [23] K. Simonyan and A. Zisserman, "Very Deep Convolutional Networks for Large-Scale Image Recognition," *Intl. Conf. Learn. Represent.*, pp. 1–14, 2015.
- [24] M. Everingham, L. Van Gool, C. K. I. Williams, J. Winn, and A. Zisserman, "The pascal visual object classes (VOC) challenge," *Int. J. Comput. Vis.*, vol. 88, no. 2, pp. 303–338, 2010.
- [25] I. Goodfellow, Y. Bengio, and A. Courville, *Deep Learning*. MIT Press, 2016.
- [26] D. P. Kingma and J. Ba, "Adam: A Method for Stochastic Optimization," pp. 1–15, 2014.
- [27] K. He, G. Gkioxari, P. Dollár, and R. Girshick, "Mask R-CNN," 2017.
- [28] L.-C. Chen, G. Papandreou, F. Schroff, and H. Adam, "Rethinking Atrous Convolution for Semantic Image Segmentation," 2017.